Control of Mesoscale Morphology and Photovoltaic Performance in Diketopyrrolopyrrole-Based Small Band Gap Terpolymers

Long Ye, Xuechen Jiao, Shaoqing Zhang, Huifeng Yao, Yunpeng Qin, Harald Ade,* and Jianhui Hou**

Morphology control is one of the key strategies in optimizing the performance of organic photovoltaic materials, particularly for diketopyrrolopyrrole (DPP)-based donor polymers. The design of DPP-based polymers that provide high power conversion efficiency (PCE) presents a significant challenge that requires optimization of both energetics and morphology. Herein, a series of high performance, small band gap DPP-based terpolymers are designed via two-step side chain engineering, namely introducing alternating short and long alkyls for reducing the domain spacing and inserting alkylthio for modulating the energy levels. The new DPP-based terpolymers are compared to delineate how the side chain impacts the mesoscale morphology. By employing the alkylthio-substituted terpolymer PBDPP-TS, the new polymer solar cell (PSC) device realizes a good balance of a high V_{oc} of 0.77 V and a high J_{sc} over 15 mA cm^{-2}, and thus realizes desirable PCE in excess of 8% and 9.5% in single junction and tandem PSC devices, respectively. The study indicates better control of domain purity will greatly improve performance of single junction DPP-based PSCs toward 10% efficiency. More significantly, the utility of this stepwise side chain engineering can be readily expanded to other classes of well-defined copolymers and triggers efficiency breakthroughs in novel terpolymers for photovoltaic and related electronic applications.

1. Introduction

Polymer solar cells (PSCs) have been actively pursued for energy-harvesting applications due to their high power to weight ratios, use of abundant elements, and flexibility. Known for its extremely electron-deficient nature and good planarity as well as scalable —three to four step synthesis, diketopyrrolopyrrole (DPP) is particularly attractive as building block in molecular design and synthesis of high performance donor (D)–acceptor (A) conjugated copolymers for PSCs with various device structures such as conventional, inverted, multiple blends, tandem, and hybrid polymer/perovskite photovoltaic devices.[1–9] Moreover, small band gap DPP-based copolymers have been selected as model materials to establish a wider range of fundamental understanding of the structure-performance and process-performance relationships in PSCs, such as the selection of primary solvent,[10–12] the choice of solvent additive,[13–15] the impact of molecular weight,[16,17] and the effect of atom[3,18] or alkyl chain substitution.[19–23] Among those DPP-containing copolymers, DPP and alkylthienyl substituted benzodithiophene (BDT-T) copolymers (abbreviated as PBDPP polymers) are regarded as one of the best choices for constructing highly efficient multiple-junction PSCs and also prototype systems to establish correlations between the structure and device performance.[24–27] Utilizing these small band gap PBDPP copolymers, Yang and co-workers promoted the power conversion efficiencies (PCEs) in excess of 6.5% and 8.5% in single and double junction PSCs, respectively.[19,24,25] Although these polymers afford excellent PCEs in double junction PSCs, previous reports have not fully exploited the potential of PBDPP polymers. Single junction PSC devices with high efficiency have not been shown yet, despite the broad spectral coverage and strong near infrared absorption band. The main obstacles limiting potential applications of small band gap PBDPP polymers is the relatively low external quantum efficiency (EQE) and high-lying highest occupied molecular orbital (HOMO) level, with typical values below 50% and –5.2 eV, respectively. As a result, few of them could simultaneously achieve high short-circuit current density (J_{sc} > 15 mA cm^{-2}) and high open-circuit voltage (V_{oc} > 0.75 V) in single junction PSCs, and thereby the PCE is generally limited at 6%–7%. Therefore, meeting the above two requirements continues to be a great challenge for the molecular design of this type of small band gap polymers.

The morphological characteristics of DPP-based polymer:phenyl-C_{71}-butyric acid methyl ester ($PC_{71}BM$) blends

Dr. L. Ye, S. Q. Zhang, H. F. Yao, Y. P. Qin, Prof. J. H. Hou
State Key Laboratory of Polymer Physics and Chemistry
Beijing National Laboratory for Molecular Sciences
Institute of Chemistry
Chinese Academy of Sciences
Beijing 100190, China
E-mail: lye4@ncsu.edu, yelong@iccas.ac.cn; hjhzlz@iccas.ac.cn
Dr. L. Ye, X. C. Jiao, Prof. H. Ade
Department of Physics and Organic and Carbon Electronics Lab (ORaCEL)
North Carolina State University
Raleigh, NC 27695, USA
E-mail: hwade@ncsu.edu

DOI: 10.1002/aenm.201601138

at the mesoscale have been recently recognized as critical factors in determining the photovoltaic parameters of PSCs.[12,22] That is to say, high performance DPP-based polymers can only be achievable with a mesoscale morphology that has a length scale close to the exciton diffusion length. Molecular design is a feasible tool to achieve this goal. For instance, Janssen and co-workers found the fibril width of DPP-based polymers can be decreased by shortening the length of alkyl chains, which afforded considerably enhanced EQE and J_{sc} accordingly.[23] Recently, Kim et al.[28] found that the crystallinity, mobility, and photovoltaic performance of DPP-based polymers could be optimized by a terpolymer approach based on three monomers, such as DPP, selenophene, and thiophene. The resulting DPP-based polymers in both cases exhibited excellent PCE values over 7%. In addition, terpolymer design strategy is a feasible strategy used to create other kinds of semiconducting polymers with tailored energy levels and optical band gaps, and optimal crystalline behaviors.[29] Applying alkyl engineering and terpolymer strategies simultaneously may lead to highly tunable morphological properties and thus greatly enhanced device performances.

In this contribution, we present that the mesoscale morphology of DPP-based polymers can be finely manipulated by a two-step molecular design strategy, i.e., a series of novel PBDPP terpolymers, by stepwise modulation of the side chains appended to the donor and acceptor units. First, the crystallinity and mesoscale morphology of the PBDPP terpolymers can be systematically controlled by tuning the ratio between short and long alkyls of DPP units. Second, optimizing the open-circuit voltage without sacrificing the other parameters by introducing alkylthio side chains in the BDT-T units. On the basis of quantum-chemical calculations, alkylthio-substituted BDT-T (BDT-TS) was expected to obtain a theoretical HOMO level ≈0.24 eV lower than the BDT-T (**Scheme 1**). In this regard, we may increase the V_{oc} of PBDPP polymer by sulfur substitution of BDT-T, which lowered HOMO level without sacrificing the high current density (J_{sc}) of the original and well-defined backbone. The impact of stepwise side chain engineering on the band gaps, the molecular energy levels, the mesoscale morphologies of the DPP-based terpolymers was investigated by means of 2D grazing incidence wide-angle X-ray scattering (GIWAXS) and resonant soft X-ray scattering (R-SoXS), and correlated well with their photovoltaic properties. More importantly, our work establishes excellent and direct correlations between morphological parameters (long period, domain purity variations) and device parameters (J_{sc}, fill factor) in new terpolymer materials, which is seldom observed before.

2. Results and Discussions

2.1. Basic Properties and Molecular Design of PBDPP-T*x* Terpolymers

A series of new PBDPP terpolymers named as PBDPP-T*x* (x = 1, 2, 3), were prepared using palladium-catalyzed cross-coupling condensation polymerization of equal BDT-T and DPP monomers, as shown in **Scheme 2**. The terpolymers were obtained in high yields (50%–60%) and full synthetic details are included in the Supporting Information. All of the PBDPP terpolymers are composed of identical backbones, but have different composition and distribution of the alkyl chains, i.e., 2-ethylhexyl (EH) and 2-octyldedecyl (OD) in DPP unit. The molecular weight of these terpolymers were determined by high temperature gel permeation chromatography using 1, 3, 5-trichlorobenzene as eluent at 140 °C. The resulting number-averaged molecular weights are M_n = 81 kg mol^{-1} for PBDPP-T1, M_n = 100 kg mol^{-1} for PBDPP-T2, and M_n = 131 kg mol^{-1} for PBDPP-T3, with similar polydispersity index (PDI) values around 4. A copolymer PBDPP-OD (M_n = 114 kg mol^{-1}, PDI = 3.6) was also synthesized as control.[26] The terpolymers exhibited moderate solubility (4–8 mg mL^{-1}) in chlorobenzene (CB) and chloroform (CF). As observed from thermogravimetric (TGA) curves, all PBDPP polymers showed a decomposition temperature over 400 °C. The UV–vis absorption spectra of the PBDPP-T*x* terpolymers were measured both in solution and thin film, as shown in **Figure 1**. Compared to the PBDPP-OD, these terpolymers exhibit a slightly red-shifted absorption maximum and absorption onset by ≈5 nm in both film and dilute solution forms. The optical band gaps (E_g^{opt}) of terpolymers are ≈1.41 eV. Cyclic voltammetry (CV) measurements were used to estimate HOMO energy levels of these terpolymers by using the onset of oxidation potential and lowest unoccupied molecular orbital (LUMO) levels were deduced by addition of E_g^{opt} to the HOMO energies. Compared with PBDPP copolymer, all of the terpolymers exhibited an identical HOMO level of –5.27 eV.

In many cases, polymer crystallinity and crystallite preferential orientation have been shown to impact charge transport within active layers.[30–32] Here, GIWAXS was used to study the molecular packing of the neat polymer films to reveal the impact of different side chains on the overall crystallinity. The in-plane and out-of-plane 15° sector averages of neat polymers are displayed in **Figure 2**. From the GIWAXS profiles, all five PBDPP-based polymers exhibit a defined π–π stacking (010) peak along out-of-plane direction, mirrored with lamellar stacking (100) peak along in-plane direction. It indicates that the beneficial face-on preferential orientation relative to the substrate remains irrespective of the side-chain engineering. The 2D GIWAXS patterns (Figure S1, Supporting Information) further verify the face-on preferential orientation of polymer crystallites. Additionally, the π–π stacking distances of all pure polymers in the out-of-plane direction are ≈3.8 Å^{-1} (**Table 1**), indicative of similar charge transport property. However, the broad (100) and (010) peaks and weak high order (h00) peaks imply that the side chain engineering employed in this study does not improve the relatively low crystallinity and low molecular ordering exhibited by PBDPP-OD.

2.2. Photovoltaic Performance and Mesoscale Morphology of PBDPP-T*x* Terpolymer

Single junction PSCs with a conventional device structure of Indium tin oxide (ITO)/Poly(3,4-ethylenedioxythiophene)-poly(styrenesulfonate) (PEDOT:PSS)/PBDPP-T*x*:$PC_{71}BM$/Mg/Al were fabricated by spin-coating of a 1:2 terpolymer:$PC_{71}BM$ blend from a chlorobenzene/1,8-diiodooctane (97/3) solvent mixture. The corresponding device performance parameters

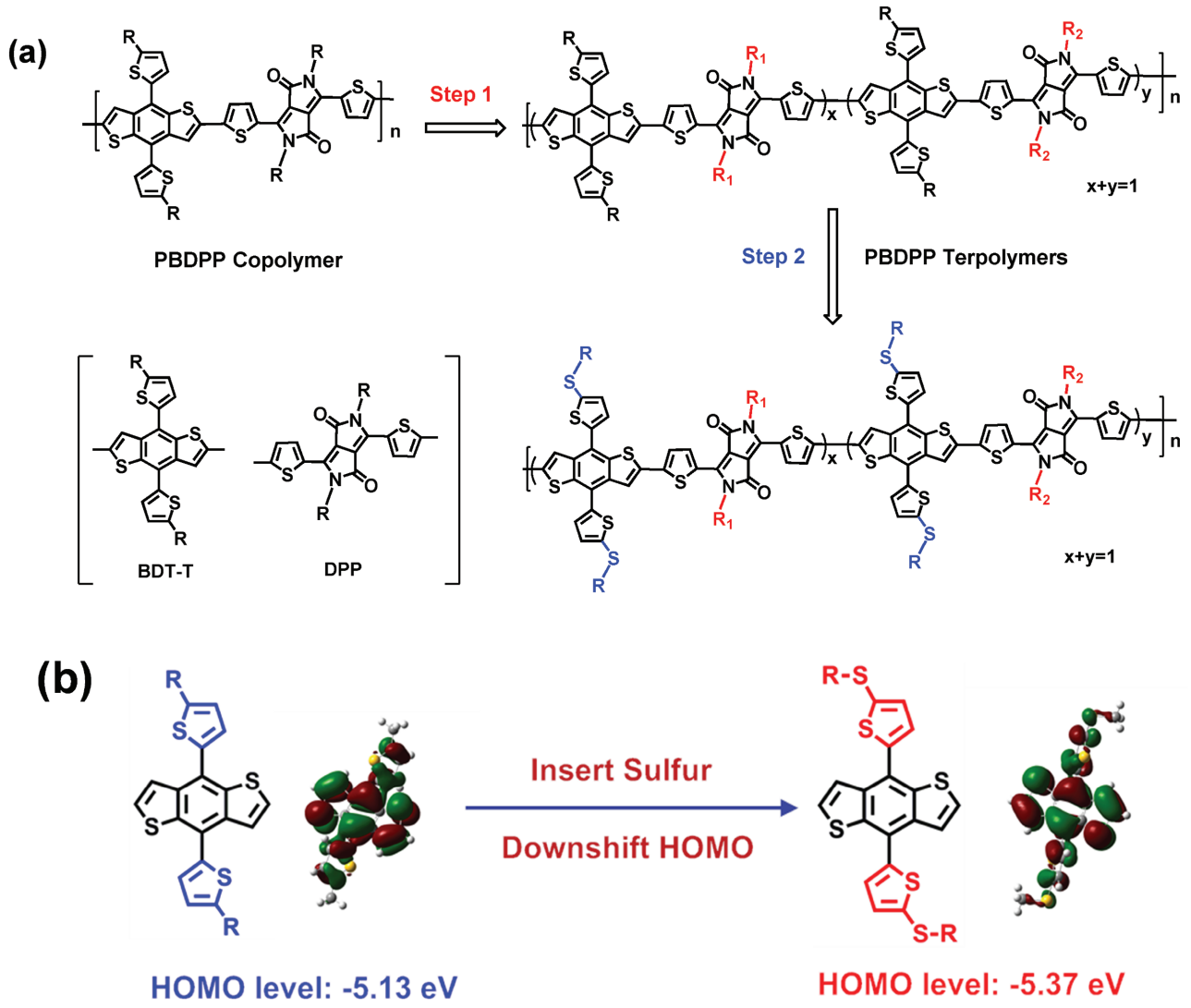

Scheme 1. a) Molecular design of DPP-based terpolymers with two-step side chain engineering starting from the PBDPP copolymer and b) the evolution of HOMO level of BDT-T unit by inserting sulfur atom.

(**Table 2**) were measured under AM 1.5G 100 mW cm^{-2} condition with the combination of Class AAA solar simulator and a KG3 filtered silicon reference cell. The difference between the J_{sc} values from *J*–*V* and EQE tests (**Figure 3**) is below 5%. Compared to the poor performance of PBDPP-OD, PBDPP-T*x* terpolymers-based PSCs showed high J_{sc} values with two-fold to threefold enhancement (see Figure 3a). The device performance of PBDPP-OD:$PC_{71}BM$ is rather poor, which indicates that better molecular ordering does not necessarily leads to good device performance. We note that the overall shape of EQE curve does not always follow the same trend with that of UV–vis absorption spectra of terpolymers, which means the relative photoresponse from PBDPP-polymer or PCBM is highly morphology dependent, mirroring similar observations in PDPP3T[12].

Atomic force microscopy (AFM) is used to study the surface morphology of these blend films (Figure S2, Supporting Information) and the corresponding surface roughness values are also indicated. PBDPP-OD:PCBM showed a rougher surface and larger length scale of phase separation from the phase image compared to the terpolymer:PCBM blends. However, there exists quite limited differences between those terpolymers with a surface roughness of 1–2 nm from the height images, though PBDPP-T1:$PC_{71}BM$ film exhibits a slightly coarser feature of aggregates. To probe the bulk, high spatial resolution from a few nanometers to several microns and contrast tunability from material contrast to mass-thickness contrast make R-SoXS one of the most quantitative tools to probe compositional domain structure of polymer composites, particularly polymer:fullerene blends.[33,34] To gain insight into the impact of alkyl chains on the bulk morphology of DPP-based terpolymers, R-SoXS was employed in a transmission geometry. R-SoXS profiles of all blends (**Figure 4**a) show well-defined peaks, corresponding to domain spacing with a long period $d = 2\pi/q$, where q is the mode of the spatial frequency distribution, of 128.0, 63.4, 43.7, and 26.8 nm for the PBDPP-OD,

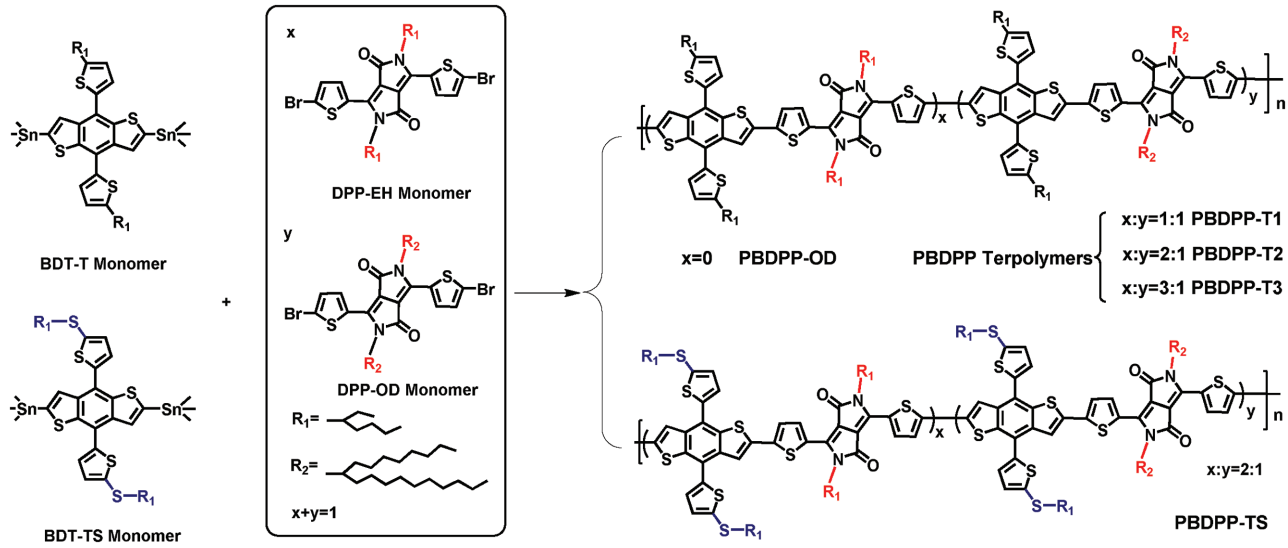

Scheme 2. Synthesis of a series of PBDPP-based terpolymers by Stille coupling.

PBDPP-T1, PBDPP-T2, and PBDPP-T3-based blend films, respectively. In comparison with the PBDPP copolymer PBDPP-OD blend, the blend films based on PBDPP-Tx terpolymers exhibit substantially reduced long periods. This observation is also verified by the transmission electron microscopy (TEM) images shown in Figure S3 (Supporting Information). In addition, the average composition variation (relative purity variations) can be extracted via the integration of R-SoXS profiles over the q range probed.[12,30,34] For the BHJ systems with a straightforward morphology, the relative domain purity variation is proportional to the square root of the integrated scattering intensity (ISI),[34] where $\mathrm{ISI} = \int I(q)q^2\mathrm{d}q$. Here, the relative domain purity variations of all blend films are normalized to the highest relative purity assigned a value of 1. The long period and relative domain purity

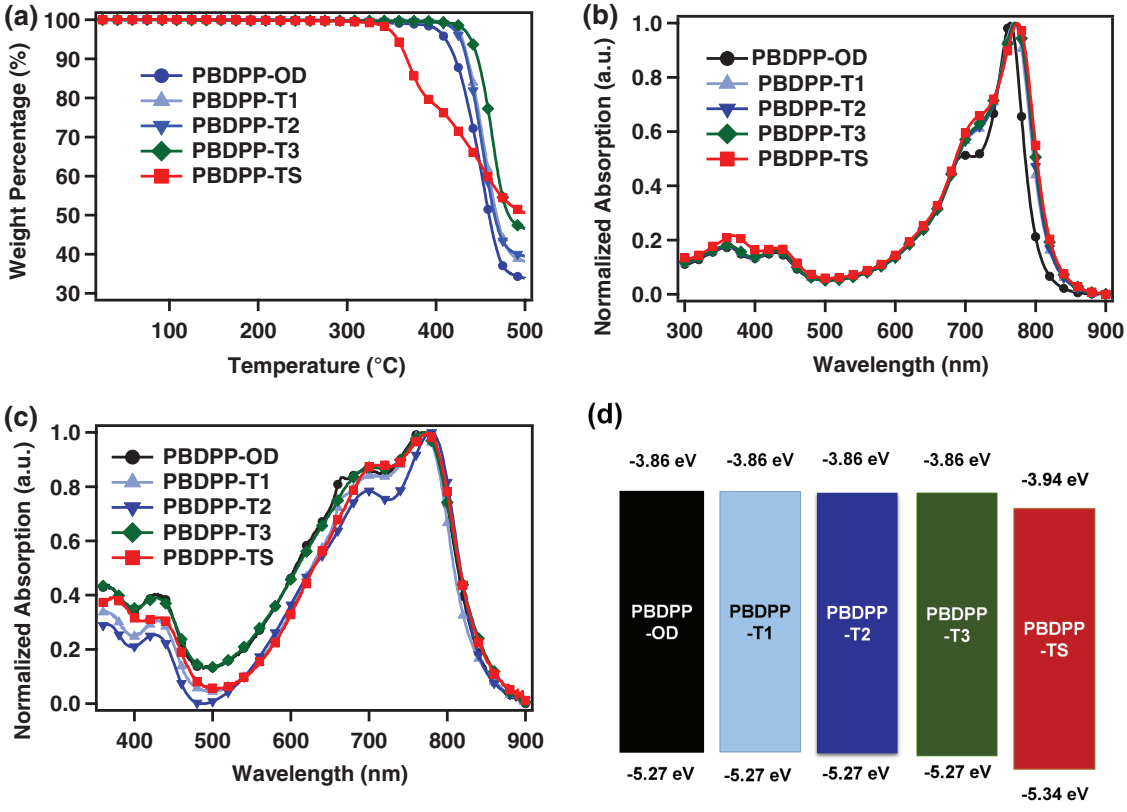

Figure 1. Basic properties of neat PBDPP polymers: a) TGA curves. Absorption spectra in b) CF solution and c) thin film. d) Energy levels.

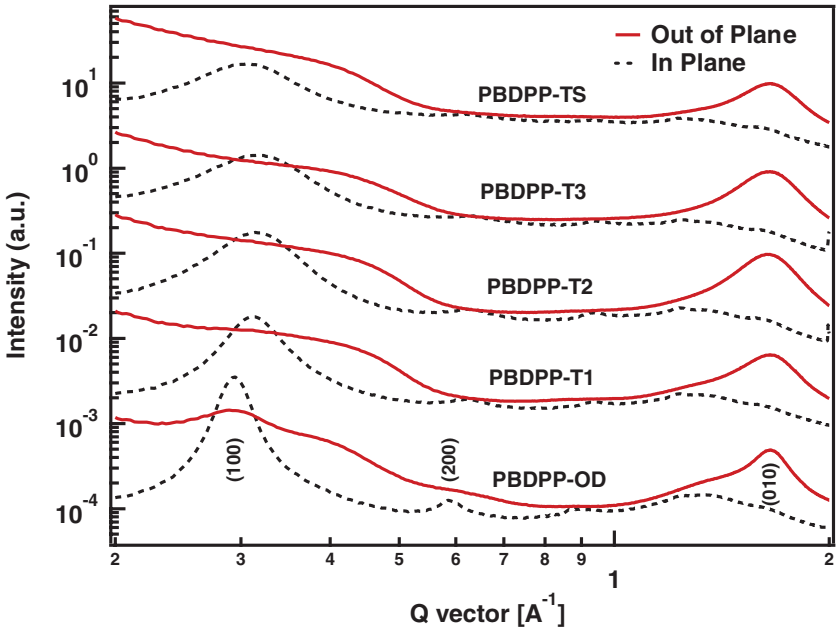

Figure 2. Out-of-plane and in-plane 15° sector average GIWAXS profiles of neat PBDPP-polymer films. The profiles of different films are offset vertically for clarity.

are tabulated in Table 2. With the increase of molar ratio of short chain (*x*), the long period (domain spacing) and relative domain purity are reduced in PBDPP-T*x* terpolymers gradually. As is well known, a small long period is beneficial for maximizing the D/A interface area and improving charge generation and thus J_{sc} when the length scale of phase separation is much higher than the typical exciton diffusion length (20 nm), while a low relative domain purity leads to a detrimental increased charge recombination and thus poor fill factor (FF).[30] Specifically, the PBDPP-T3:PCBM blend has on average more impure domain than PBDPP-OD:PCBM blend yet a very small long period of 26.8 nm, which is approaching the optimum length scale on the order of the exciton diffusion length, consistent with its enhanced EQE (Figure 3b). Accordingly, a highest J_{sc} and lowest FF are observed in PBDPP-T3-based PSC. In contrast, a highest FF and lowest J_{sc} are recorded in PSC based on PBDPP-T1. Owing to the optimized trade-off between J_{sc} and FF, PBDPP-T2 with a monomer ratio of 2:1 is the highest performing one in the above-mentioned PBDPP-T*x* terpolymers.

2.3. Device Performance and Molecular Design of PBDPP-TS

In searching for an ideal small band gap DPP-based material, we further engineer the side chain of BDT-T unit of PBDPP-T2. According to our and other recent studies, insertion of alkylthio chain is a feasible strategy to downshift the HOMO levels and meliorate the photovoltaic performances of BDT-T containing polymers.[35,36] Consequently, alkylthio was introduced to optimize the molecular structure of PBDPP-T2, and a novel terpolymer PBDPP-TS were synthesized with a number-averaged molecular weight (M_n) of 77.3 kg mol^{-1} and a PDI of 4.20, as shown in Scheme 2. PBDPP-TS exhibited a slightly lower band gap of 1.40 eV and a preferred face-on orientation (see Figure S1, Supporting Information). As expected, the HOMO level of PBDPP-TS was downshifted by ≈0.1 eV when compared with PBDPP-T2, and thus improved V_{oc} can be anticipated in PBDPP-TS:$PC_{71}BM$-based PSCs. The surface image of PBDPP-TS:$PC_{71}BM$ blend film as revealed by AFM characterization (Figure S2, Supporting Information) shows a relatively small roughness of 0.96 nm. As illustrated from the R-SoXS profile (Figure 4a) and TEM image (Figure 4b) of PBDPP-TS:$PC_{71}BM$ blend film, we find its domain purity (0.93 ± 0.01) is almost identical to that of PBDPP-T2:$PC_{71}BM$ and the long period (domain length scale) is slightly lower, so the J_{sc} of PBDPP-TS device is slightly increased to 15.7 mA cm^{-2}. Given the tunability of long period and the exceptional single junction performance, PBDPP terpolymers may become the material of choice for the implementation of normal PSC device in a wide range of applications, such as ternary blend and multijunction PSCs. For instance, the synergetic side chain engineering makes the fine-tuned terpolymer PBDPP-TS fully meet the above requirements for high-performance, small band gap DPP-based polymers. Remarkably, the simultaneously high V_{oc} of 0.77 V and high J_{sc} of 15.7 mA cm^{-2} in PBDPP-TS system are rarely achieved in its copolymer analog for such a low band gap of 1.4 eV. Compared with the device parameters of other high performance DPP-based copolymers reported previously, the synergisticly high V_{oc} and J_{sc} make our newly designed PBDPP-based terpolymers more amenable for high performance tandem device fabrication. To further explore the potential of PBDPP-TS in photovoltaic devices, PBDPP-TS:$PC_{71}BM$ blend was further used as a red-absorber in double junction PSC. Using our recently developed large band gap polythiophene derivative PBDD4T-2F and $PC_{61}BM$ blend as a front cell[37] and PBDPP-TS:$PC_{71}BM$ as a rear cell afford a 9.5% efficiency tandem PSC with a V_{oc} of

Table 1. Optical properties and molecular energy levels of the PBDPP terpolymers and PDPP-OD.

Polymer	$\lambda_{peak}/\lambda_{edge}$ solution [nm]	$\lambda_{peak}/\lambda_{edge}$ film [nm]	E_g [eV]	HOMO [eV]	LUMO [eV]	$d_{(010)}$ [Å]
PBDPP-OD	765/810	770/880	1.41	−5.27	−3.86	3.79
PBDPP-T1	770/830	775/880	1.41	−5.27	−3.86	3.80
PBDPP-T2	770/830	775/880	1.41	−5.27	−3.86	3.82
PBDPP-T3	770/830	775/880	1.41	−5.27	−3.86	3.81
PBDPP-TS	775/835	775/885	1.40	−5.34	−3.94	3.80

Table 2. Photovoltaic parameters of the conventional PSCs based on the blends of PBDPP-based polymer:$PC_{71}BM$.

Polymer	V_{oc} [V]	J_{sc}[a] [mA cm^{-2}]	FF	$PCE_{max(ave)}$ [%]	Long period [nm]	Domain purity[b] [±0.01]
PBDPP-OD	0.74	4.3 (4.0)	0.67	2.13 (1.9)	128.0	1.00
PBDPP-T1	0.71	12.6 (12.5)	0.64	5.82 (5.6)	63.4	0.95
PBDPP-T2	0.71	15.5 (15.8)	0.65	7.19 (7.0)	43.7	0.94
PBDPP-T3	0.71	17.3 (17.3)	0.58	7.03 (6.8)	26.8	0.79
PBDPP-TS	0.77	15.7 (16.0)	0.64	8.04 (7.8)	35.7	0.93

[a]The values estimated from EQE data are shown in the parentheses; [b]The error bars are displayed in the brackets.

1.65 V, a J_{sc} of 10.0 mA cm^{-2}, and a FF of 57.4% (see Figure S4, Supporting Information). This result therefore exemplifies the great benefits of the simultaneous optimization of domain purity variation and long period of PBDPP-TS.

2.4. Direct Correlations of Morphological and Device Parameters

In order to further quantify the relationship between device performance and morphological parameters extracted from R-SoXS, plots of J_{sc} versus dominant domain spacing and FF versus relative domain purity are displayed in Figure 4c,d, respectively. Remarkably, linear correlations are found in both plots, i.e., purer domain contributes to higher FF and smaller domain results in higher J_{sc} in this class of PBDPP polymers. The precise reason for such linearity are currently not known and require additional study to understand. FF generally depends on a number of factors, such as mobility and bimoleculer recombination coefficient, which in turn depends on the current density and domain purity. Regarding J_{sc} and considering round fibrils, the interfacial area is proportional to the diameter. If J_{sc} is limited by the exciton harvesting, indeed, J_{sc} should show a linear relation with long period if the spacing of fibrils scales with its diameter. In the diagram of three phase morphology including relatively pure donor aggregates, relatively pure acceptor aggregates, and amorphous intermixed phase, too high average composition variation in the amorphous intermixed phase can induce fullerene composition below the percolation threshold,[30,38] which may also lead to more trapped charges and low performance if there is insufficient number of percolating pathways in the mixed regions.

Indeed, the J_{sc}–long period correlation in our study is consistent with the previous trend that smaller fibrillar width leads to higher EQE and J_{sc} in other DPP-based copolymers as observed by Janssen and co-workers using TEM.[23] The results presented above established that the mesoscale morphology can be highly manipulated by side chain engineering in a new class of PBDPP terpolymers. Considering that the long period changes considerably and anticorrelates with J_{sc} without much deviation from linearity, higher J_{sc} over 20 mA cm^{-2} may be possible if the long period decreases to 20 nm or below. Simultaneous control over purity would further improve the performance. It is noteworthy that all of the R-SoXS profiles are completely dominated by a single log-normal distribution and this is the first time that such high correlations have been reported for J_{sc} and FF. Our PBDPP terpolymer might be a superb and simple model system to understand the morphology creation and its impact. Clearly, these PBDPP terpolymers with different alkyl chains have different Hansen solubility parameters[39] and thus exhibit likely different miscibility with the fullerene, similar to the differences observed for PSBTBT-08:fullerenes.[40] The molecular interactions of donor:acceptor pairs may be the fundamental factor dominating the phase purity and thus morphology and performance.

3. Conclusions

In summary, we demonstrate a two-step side chain engineering strategy to significantly improve the mesoscale morphology and device performance of PBDPP copolymers. A series of new PBDPP terpolymers were designed, synthesized, and

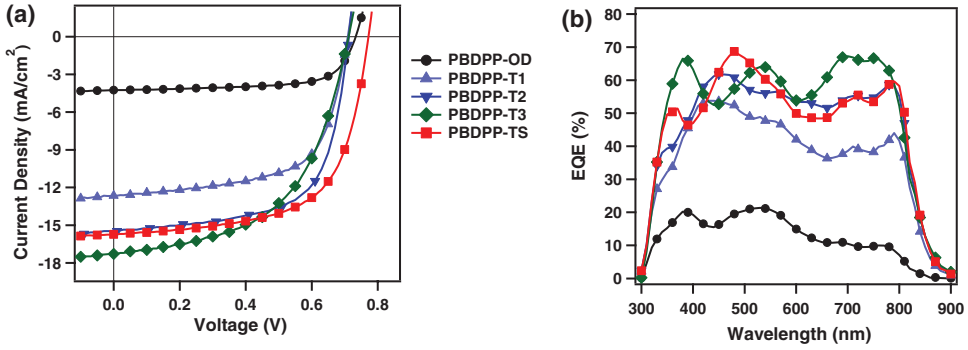

Figure 3. a) *J–V* and b) EQE curves of the PSCs based on PBDPP-OD and PBDPP-based terpolymers. $PC_{71}BM$ was used as electron acceptor.

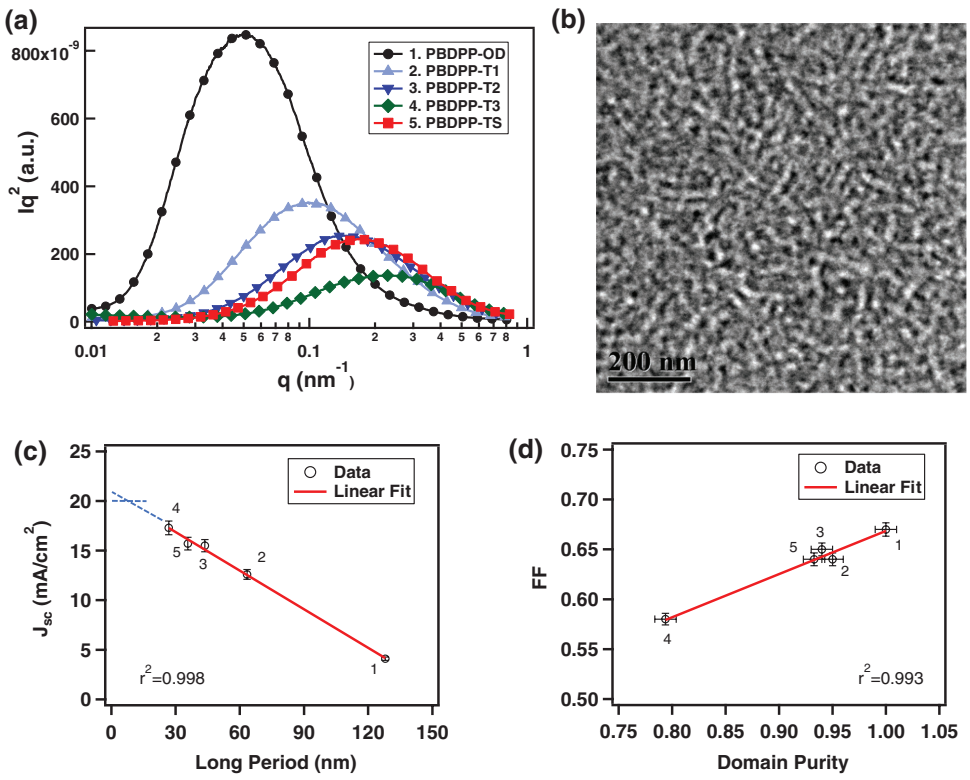

Figure 4. a) Thickness normalized and Lorentz corrected R-SoXS profiles of various blend films of PBDPP-OD and PBDPP terpolymers. b) TEM image of PBDPP-TS:$PC_{71}BM$ blend film. c) Plot of the J_{sc} of PSCs for PBDPP-based polymers versus the respective average long period obtained from R-SoXS. d) Plot of FFs of PSCs for PBDPP-based polymers versus the respective domain purities obtained from R-SoXS. The correlation coefficients (*R*-squared) of both plots are also indicated. The dashed lines in Figure 4c are added to estimate the long period for a higher J_{sc} above 20 mA cm^{-2}.

characterized. We found that domain purity correlates positively with the device FF. In contrast, J_{sc} has a reciprocal relationship with long period in this class of terpolymers. Remarkably, an alkylthio-substituted terpolymer PBDPP-TS afforded a high PCE of ≈8% and ≈9.5% in single and double junction PSCs, respectively, which is seldom achieved in the copolymer analog for such a low band gap of 1.4 eV. The exceptional photovoltaic performance of PBDPP-TS is ascribed to the relatively small characteristic domain spacing and high average relative domain purity as evidenced by R-SoXS characterizations. We also speculate that better control of purity will greatly improve performance of single junction DPP-based PSCs toward 10% efficiency. Although the stepwise side chain engineering has been exemplified with PBDPP copolymers, its utility can be easily expanded to other kinds of well-defined copolymers and triggers efficiency breakthroughs in novel terpolymers for photovoltaic and related electronic applications.

4. Experimental Section

Materials: The synthesis details of the monomers (BDT-T, BDT-TS) could be found in the previous reports.[26,35] The monomers (DPP-EH, DPP-OD) used in the synthesis of the terpolymers were purchased from Solarmer Energy Inc. Details of the synthesis of terpolymers were described in the Supporting Information. The synthetic details of PBDD4T-2F could be found in a recent work.[37] The PEDOT:PSS (P VP AI 4083) and electrode materials (purity >99%) were commercially available products and used without any further purification.

Fabrication and Characterization of PSC Devices: Polymer:$PC_{71}BM$ blends (1:2 by weight) were prepared using the same procedures as the previous report[35] with a conventional ITO/PEDOT:PSS/active layer/Mg (20 nm)/Al (100 nm) structure. A polymer concentration of 5 mg mL^{-1} in chlorobenzene was adopted and 3% (volume) 1,8-diiodooctane was used as solvent additive. The active layer thickness was ≈110 nm as measured by a Bruker Dektak XT profilometer. Five pixels, each with an active area of 4.15 mm^2 were fabricated per ITO substrate (1.5 cm × 1.5 cm). The current density–voltage (*J*–*V*) characteristics were measured under a Keithley 2400 Source Measure Unit under AM 1.5G 100 mW cm^{-2} by the AAA grade XES-70S1 solar simulator (SAN-EI Electric Co., Ltd.). The mismatch factors (MMFs) were calibrated by using silicon reference cell with KG3-filter according to the previous work.[41] The space-charge-limited current current–voltage characteristics of the hole-only diodes were measured in the dark ambient conditions. Except for the deposition of the PEDOT:PSS layers, all the fabrication processes were carried out in a nitrogen glovebox containing less than 5 ppm O_2 and H_2O. The EQE curves were measured by the use of the Enli QE-R3011 Measurement System (Enli Tech Inc, Taiwan), and the light intensity at each wavelength was calibrated with a standard single crystal silicon photovoltaic cell. The electrochemical CV was conducted on a Chi650D instrument with glassy carbon disk, Pt wire, and Ag/Ag^+ electrode as the working electrode, counter electrode, and reference electrode, respectively, in a 0.1 M tetrabutylammonium hexafluorophosphate (n-Bu_4NPF_6)-anhydrous acetonitrile solution at a potential scan rate of 50 mV s^{-1}. The device fabrication details of double junction devices were shown in the Supporting Information.

Instrumentation: GIWAXS, R-SoXS, and reference near-edge X-ray absorption fine-structure (NEXAFS) spectroscopy measurements were performed at beamline 7.3.3,[42] beamline 11.0.1.2,[43] and beamline 5.3.2.2,[44,45] respectively, at the Advanced Light Source, Lawrence

Berkeley National Laboratory, Berkeley, CA following the previously established protocols.

Supporting Information

Supporting Information is available from the Wiley Online Library or from the author.

Acknowledgements

L.Y. and X.C.J. contributed equally to this work. The authors gratefully acknowledge the financial support from the NSFC (21325419, 91333204), the CAS-Croucher Fund for Joint Lab (CAS14601), and the Chinese Academy of Science (XDB12030200, KJZD-EW-J01). X-ray data acquisition and analysis by X.C.J., L.Y., and H.A. were supported by the ONR grant N00141512322. X-ray data were acquired at the Advanced Light Source, which was supported by the Director, Office of Science, Office of Basic Energy Sciences of the U.S. Department of Energy under Contract No. DE-AC02-05CH11231. The authors thank C. Wang, C. Zhu, A.L.D. Kilcoyne, E. Schaible, A. Hexemer, Y. Yu, and A. Young of the ALS (DOE) for helping with the synchrotron experimental set-up and maintenance of the beamlines.

Received: May 30, 2016
Revised: September 1, 2016
Published online: October 26, 2016

[1] a) L. Dou, Y. Liu, Z. Hong, G. Li, Y. Yang, *Chem. Rev.* **2015**, *115*, 12633; b) S. Qu, H. Tian, *Chem. Commun.* **2012**, *48*, 3039; c) H. Yao, L. Ye, H. Zhang, S. Li, S. Zhang, J. Hou, *Chem. Rev.* **2016**, *116*, 7397.

[2] W. Li, K. H. Hendriks, M. M. Wienk, R. A. J. Janssen, *Acc. Chem. Res.* **2016**, *49*, 78.

[3] R. S. Ashraf, I. Meager, M. Nikolka, M. Kirkus, M. Planells, B. C. Schroeder, S. Holliday, M. Hurhangee, C. B. Nielsen, H. Sirringhaus, I. McCulloch, *J. Am. Chem. Soc.* **2015**, *137*, 1314.

[4] a) J. W. Jung, F. Liu, T. P. Russell, W. H. Jo, *Energy Environ. Sci.* **2013**, *6*, 3301; b) Q. Peng, Q. Huang, X. Hou, P. Chang, J. Xu, S. Deng, *Chem. Commun.* **2012**, *48*, 11452.

[5] Y. Yang, W. Chen, L. Dou, W.-H. Chang, H.-S. Duan, B. Bob, G. Li, Y. Yang, *Nat. Photonics* **2015**, *9*, 190.

[6] a) Y. Liu, Z. Hong, Q. Chen, W. Chang, H. Zhou, T.-B. Song, E. Young, Y. Yang, J. You, G. Li, Y. Yang, *Nano Lett.* **2015**, *15*, 662; b) C. T. Zuo, L. M. Ding, *J. Mater. Chem. A* **2015**, *3*, 9063; c) L. Ye, B. Fan, S. Zhang, S. Li, B. Yang, Y. Qin, H. Zhang, J. Hou, *Sci. China Mater.* **2015**, *58*, 953; d) J. Kim, G. Kim, H. Back, J. Kong, I. W. Hwang, T. K. Kim, S. Kwon, J. H. Lee, J. Lee, K. Yu, C. L. Lee, H. Kang, K. Lee, *Adv. Mater.* **2016**, *28*, 3159.

[7] a) C.-C. Chen, S.-H. Bae, W.-H. Chang, Z. Hong, G. Li, Q. Chen, H. Zhou, Y. Yang, *Mater. Horiz.* **2015**, *2*, 20; b) J. Liu, S. Lu, L. Zhu, X. Li, W. C. H. Choy, *Nanoscale* **2016**, *8*, 3638; c) Y. Zhang, W. Yu, W. Qin, Z. Yang, D. Yang, Y. Xing, S. Liu, C. Li, *Nano Energy* **2016**, *20*, 126.

[8] a) K. Li, Z. Li, K. Feng, X. Xu, L. Wang, Q. Peng, *J. Am. Chem. Soc.* **2013**, *135*, 13549; b) J. Jo, J.-R. Pouliot, D. Wynands, S. D. Collins, J. Y. Kim, T. L. Nguyen, H. Y. Woo, Y. Sun, M. Leclerc, A. J. Heeger, *Adv. Mater.* **2013**, *25*, 4783.

[9] a) J. Gilot, M. M. Wienk, R. A. J. Janssen, *Adv. Mater.* **2010**, *22*, E67; b) W. Li, K. H. Hendriks, A. Furlan, W. S. C. Roelofs, M. M. Wienk, R. A. J. Janssen, *J. Am. Chem. Soc.* **2013**, *135*, 18942; c) H. Tan, A. Furlan, W. Li, K. Arapov, R. Santbergen, M. M. Wienk, M. Zeman, A. H. M. Smets, R. A. J. Janssen, *Adv. Mater.* **2016**, *28*, 2170.

[10] J. C. Bijleveld, V. S. Gevaerts, D. Di Nuzzo, M. Turbiez, S. G. J. Mathijssen, D. M. de Leeuw, M. M. Wienk, R. A. J. Janssen, *Adv. Mater.* **2010**, *22*, E242.

[11] F. Liu, Y. Gu, C. Wang, W. Zhao, D. Chen, A. L. Briseno, T. P. Russell, *Adv. Mater.* **2012**, *24*, 3947.

[12] a) L. Ye, S. Q. Zhang, W. Ma, B. H. Fan, X. Guo, Y. Huang, H. Ade, J. H. Hou, *Adv. Mater.* **2012**, *24*, 6335; b) W. Ma, J. R. Tumbleston, L. Ye, C. Wang, J. Hou, H. Ade, *Adv. Mater.* **2014**, *26*, 4234.

[13] C. H. Woo, P. M. Beaujuge, T. W. Holcombe, O. P. Lee, J. M. J. Frechet, *J. Am. Chem. Soc.* **2010**, *132*, 15547.

[14] J. J. van Franeker, M. Turbiez, W. Li, M. M. Wienk, R. A. Janssen, *Nat. Commun.* **2015**, *6*, 6229.

[15] H. Choi, S.-J. Ko, T. Kim, P.-O. Morin, B. Walker, B. H. Lee, M. Leclerc, J. Y. Kim, A. J. Heeger, *Adv. Mater.* **2015**, *27*, 3318.

[16] a) Z. Huang, E. C. Fregoso, S. Dimitrov, P. S. Tuladhar, Y. W. Soon, H. Bronstein, I. Meager, W. Zhang, I. McCulloch, J. R. Durrant, *J. Mater. Chem. A* **2014**, *2*, 19282; b) M. H. Hoang, D. N. Nguyen, T. T. Ngo, H. A. Um, M. J. Cho, D. H. Choi, *Polymer* **2016**, *83*, 77.

[17] K. H. Hendriks, G. H. L. Heintges, V. S. Gevaerts, M. M. Wienk, R. A. J. Janssen, *Angew. Chem., Int. Ed.* **2013**, *52*, 8341.

[18] a) T. Ma, K. Jiang, S. Chen, H. Hu, H. Lin, Z. Li, J. Zhao, Y. Liu, Y.-M. Chang, C.-C. Hsiao, H. Yan, *Adv. Energy Mater.* **2015**, *5*, 1501282; b) Z. Zeng, Y. Li, J. Deng, Q. Huang, Q. Peng, *J. Mater. Chem. A* **2014**, *2*, 653.

[19] A. T. Yiu, P. M. Beaujuge, O. P. Lee, C. H. Woo, M. F. Toney, J. M. J. Frechet, *J. Am. Chem. Soc.* **2012**, *134*, 2180.

[20] a) L. T. Dou, J. Gao, E. Richard, J. B. You, C. C. Chen, K. C. Cha, Y. J. He, G. Li, Y. Yang, *J. Am. Chem. Soc.* **2012**, *134*, 10071; b) L. T. Dou, W. H. Chang, J. Gao, C. C. Chen, J. B. You, Y. Yang, *Adv. Mater.* **2013**, *25*, 825.

[21] J. Yao, C. Yu, Z. Liu, H. Luo, Y. Yang, G. Zhang, D. Zhang, *J. Am. Chem. Soc.* **2016**, *138*, 173.

[22] W. Li, K. H. Hendriks, A. Furlan, W. S. C. Roelofs, M. M. Wienk, R. A. J. Janssen, *J. Am. Chem. Soc.* **2013**, *135*, 18942.

[23] W. Li, K. H. Hendriks, A. Furlan, W. S. C. Roelofs, S. C. J. Meskers, M. M. Wienk, R. A. J. Janssen, *Adv. Mater.* **2014**, *26*, 1565.

[24] L. T. Dou, J. B. You, J. Yang, C. C. Chen, Y. J. He, S. Murase, T. Moriarty, K. Emery, G. Li, Y. Yang, *Nat. Photonics* **2012**, *6*, 180.

[25] J. Gao, L. Dou, W. Chen, C.-C. Chen, X. Guo, J. You, B. Bob, W.-H. Chang, J. Strzalka, C. Wang, G. Li, Y. Yang, *Adv. Energy Mater.* **2013**, *4*, 1300739.

[26] a) S. Zhang, L. Ye, Q. Wang, Z. Li, X. Guo, L. Huo, H. Fan, J. Hou, *J. Phys. Chem. C* **2013**, *117*, 9550; b) L. Ye, S. Zhang, L. Huo, M. Zhang, J. Hou, *Acc. Chem. Res.* **2014**, *47*, 1595.

[27] a) Y. Li, C.-Y. Chang, Y. Chen, Y. Song, C.-Z. Li, H.-L. Yip, A. K. Y. Jen, C. Li, *J. Mater. Chem. C* **2013**, *1*, 7526; b) T. E. Kang, H.-H. Cho, H. J. Kim, W. Lee, H. Kang, B. J. Kim, *Macromolecules* **2013**, *46*, 6806.

[28] K.-H. Kim, S. Park, H. Yu, H. Kang, I. Song, J. H. Oh, B. J. Kim, *Chem. Mater.* **2014**, *26*, 6963.

[29] a) T. E. Kang, K.-H. Kim, B. J. Kim, *J. Mater. Chem. A* **2014**, *2*, 15252; b) T. E. Kang, H.-H. Cho, H. J. Kim, W. Lee, H. Kang, B. J. Kim, *Macromolecules* **2013**, *46*, 6806; c) Y. Huang, M. Zhang, H. Chen, F. Wu, Z. Cao, L. Zhang, S. Tan, *J. Mater. Chem. A* **2014**, *2*, 5218; d) T. Qin, W. Zajaczkowski, W. Pisula, M. Baumgarten, M. Chen, M. Gao, G. Wilson, C. D. Easton, K. Müllen, S. E. Watkins, *J. Am. Chem. Soc.* **2014**, *136*, 6049.

[30] a) S. Mukherjee, C. M. Proctor, J. R. Tumbleston, G. C. Bazan, T.-Q. Nguyen, H. Ade, *Adv. Mater.* **2015**, *27*, 1105; b) S. Mukherjee, X. Jiao, H. Ade, *Adv. Energy Mater.* **2016**, *6*, 1600699.

[31] M. Schubert, B. A. Collins, H. Mangold, I. A. Howard, W. Schindler, K. Vandewal, S. Roland, J. Behrends, F. Kraffert, R. Steyrleuthner,

Z. Chen, K. Fostiropoulos, R. Bittl, A. Salleo, A. Facchetti, F. Laquai, H. W. Ade, D. Neher, *Adv. Funct. Mater.* **2014**, *24*, 4068.

[32] a) C. Cabanetos, A. El Labban, J. A. Bartelt, J. D. Douglas, W. R. Mateker, J. M. J. Frechet, M. D. McGehee, P. M. Beaujuge, *J. Am. Chem. Soc.* **2013**, *135*, 4656; b) M. S. Chen, O. P. Lee, J. R. Niskala, A. T. Yiu, C. J. Tassone, K. Schmidt, P. M. Beaujuge, S. S. Onishi, M. F. Toney, A. Zettl, J. M. J. Fréchet, *J. Am. Chem. Soc.* **2013**, *135*, 19229.

[33] a) J. Huang, J. H. Carpenter, C.-Z. Li, J.-S. Yu, H. Ade, A. K. Y. Jen, *Adv. Mater.* **2016**, *28*, 967; b) J. Zhao, Y. Li, G. Yang, K. Jiang, H. Lin, H. Ade, W. Ma, H. Yan, *Nat. Energy* **2016**, *1*, 15027.

[34] a) B. A. Collins, Z. Li, J. R. Tumbleston, E. Gann, C. R. McNeill, H. Ade, *Adv. Energy Mater.* **2013**, *3*, 65; b) J. H. Carpenter, A. Hunt, H. Ade, *J. Electron Spectrosc. Relat. Phenom.* **2015**, *200*, 2; c) L. Ye, X. Jiao, W. Zhao, S. Zhang, H. Yao, S. Li, H. Ade, J. Hou, *Chem. Mater.* **2016**, *28*, 6178.

[35] a) L. Ye, S. Zhang, W. Zhao, H. Yao, J. Hou, *Chem. Mater.* **2014**, *26*, 3603; b) L. Ye, K. Sun, W. Jiang, S. Zhang, W. Zhao, H. Yao, Z. Wang, J. Hou, *ACS Appl. Mater. Interfaces* **2015**, *7*, 9274; c) L. Ye, X. Jiao, H. Zhang, S. Li, H. Yao, H. Ade, J. Hou, *Macromolecules* **2015**, *48*, 7156.

[36] a) C. Cui, W.-Y. Wong, Y. Li, *Energy Environ. Sci.* **2014**, *7*, 2276; b) J. W. Jung, F. Liu, T. P. Russell, W. H. Jo, *Adv. Mater.* **2015**, *27*, 7462; c) K. Feng, X. Xu, Z. Li, Y. Li, K. Li, T. Yu, Q. Peng, *Chem. Commun.* **2015**, *51*, 6290; d) X. Xu, Z. Li, Z. Wang, K. Li, K. Feng, Q. Peng, *Nano Energy* **2016**, *25*, 170.

[37] S. Zhang, Y. Qin, M. A. Uddin, B. Jang, W. Zhao, D. Liu, H. Y. Woo, J. Hou, *Macromolecules* **2016**, *49*, 2993.

[38] D. Leman, M. A. Kelly, S. Ness, S. Engmann, A. Herzing, C. Snyder, H. W. Ro, R. J. Kline, D. M. DeLongchamp, L. J. Richter, *Macromolecules* **2015**, *48*, 383.

[39] J. A. Bartelt, Z. M. Beiley, E. T. Hoke, W. R. Mateker, J. D. Douglas, B. A. Collins, J. R. Tumbleston, K. R. Graham, A. Amassian, H. Ade, J. M. J. Frechet, M. F. Toney, M. D. McGehee, *Adv. Energy Mater.* **2013**, *3*, 364.

[40] B. A. Collins, Z. Li, C. R. McNeill, H. Ade, *Macromolecules* **2011**, *44*, 9747.

[41] L. Ye, C. Zhou, H. Meng, H.-H. Wu, C.-C. Lin, H.-H. Liao, S. Zhang, J. Hou, *J. Mater. Chem. C* **2015**, *3*, 564.

[42] A. Hexemer, W. Bras, J. Glossinger, E. Schaible, E. Gann, R. Kirian, A. MacDowell, M. Church, B. Rude, H. Padmore, *J. Phys.: Conf. Ser.* **2010**, *247*, 012007.

[43] E. Gann, A. T. Young, B. A. Collins, H. Yan, J. Nasiatka, H. A. Padmore, H. Ade, A. Hexemer, C. Wang, *Rev. Sci. Instrum.* **2012**, *83*, 045110.

[44] A. L. D. Kilcoyne, T. Tyliszczak, W. F. Steele, S. Fakra, P. Hitchcock, K. Franck, E. Anderson, B. Harteneck, E. G. Rightor, G. E. Mitchell, A. P. Hitchcock, L. Yang, T. Warwick, H. Ade, *J. Synchrotron Radiat.* **2003**, *10*, 125.

[45] B. A. Collins, H. Ade, *J. Electron Spectrosc. Relat. Phenom.* **2012**, *185*, 119.